PROCEEDINGS OF SCIENCE

Searching for evidence of PeVatron activity from stellar clusters via gamma-ray and neutrino signatures

A. M. W. Mitchell,[a,*] **S. Celli,**[b,c,d] **A. Specovius,**[a] **G. Morlino**[e] **and S. Menchiari**[e,f]

[a] *Friedrich-Alexander-Universität Erlangen-Nürnberg, Erlangen Centre for Astroparticle Physics Nikolaus-Fiebiger-Str. 2, 91058 Erlangen, Germany*

[b] *Sapienza Università di Roma, Piazzale Aldo Moro 5, 00185, Rome, Italy*

[c] *Istituto Nazionale di Fisica Nucleare, Sezione di Roma, Piazzale Aldo Moro 5, 00185, Rome, Italy*

[d] *Istituto Nazionale di Astrofisica, Osservatorio Astronomico di Roma, Monte Porzio Catone, Rome, Italy*

[e] *Istituto Nazionale di Astrofisica, Osservatorio Astrofisico di Arcetri, L.go E. Fermi 5, Firenze, Italy*

[f] *INFN - Sezione di Pisa, Edificio C – Polo Fibonacci Largo B. Pontecorvo, 3 – 56127 Pisa*

E-mail: alison.mw.mitchell@fau.de

Young and massive stellar clusters are a promising source class for the acceleration of galactic cosmic rays to PeV energies. Supernova explosions of massive stars lead to semi-continuous injection of cosmic rays into the cluster environment. Collective stellar winds form a wind-blown bubble with a termination shock at which further particle acceleration may occur. Interactions of such energetic hadronic particles with target material - such as molecular clouds - will generate signature gamma-ray and neutrino emission. We apply a model of cosmic ray acceleration in stellar clusters to catalogues of known stellar clusters, identifying the most promising targets to search for evidence of PeVatron activity. Predictions for the secondary fluxes of gamma-ray and neutrino emission are derived based on particle acceleration at the collective wind termination shock. Our results are compared to data available from the H.E.S.S. Galactic Plane Survey, and we estimate the detection prospects for current and future generation neutrino experiments.

38th International Cosmic Ray Conference (ICRC2023)
26 July - 3 August, 2023
Nagoya, Japan

ICRC2023
38th International Cosmic Ray Conference
The Astroparticle Physics Conference

*Speaker

PoS(ICRC2023)611

1. Introduction

In recent years, very-high-energy ($E > 100\,\mathrm{GeV}$) γ-ray astronomy has begun detecting sources reaching γ-ray energies above 100 TeV [1]. Whether produced through hadronic mechanisms such as neutral pion-decay or leptonic mechanisms such as inverse Compton scattering, the parent particle population must have energies $\gtrsim 1$ PeV. This implies that the astrophysical particle accelerators are 'PeVatrons', the long sought-after sources responsible for Cosmic Rays (CRs) up to and beyond the so-called 'knee' feature occurring in the CR spectrum at ~ 3 PeV. Whilst supernova remnants have long been considered prime PeVatron candidates, due to theoretical and observational difficulties in reconciling such a scenario, attention has recently turned to other candidate source classes, such as stellar clusters.

Young stellar clusters drive a collective wind into the surrounding medium, producing a Wind Termination Shock at which particle acceleration can occur. Beyond this distance, a wind blown bubble further expands into the surrounding interstellar medium, a scenario depicted schematically in figure 1. In this work, we use the model of [2] to predict the expected γ-ray (and neutrino) emission from the wind-blown bubble associated with stellar clusters. We investigate how the expected spectral energy distributions depend on properties of the stellar cluster, subsequently applying the model to known stellar clusters as listed in either the Milky Way Stellar Cluster (MWSC) catalogue, or the open cluster sample from the Gaia DR2 [3, 4]. The systems with the highest predicted energy flux are then listed in ranked order and compared to available data, to generate a list of possible PeVatron candidates. Such a target list can be used to motivate future observations, to either constrain or verify the predictions of this model.

2. Properties of Stellar Clusters

A stellar cluster of radius R_c is thought to drive a wind into the surrounding ISM of density ρ, resulting in both a termination shock of the cluster wind with radius R_s and a forward shock of the wind-blown bubble with radius R_b. These are expected to depend on the age of the stellar cluster t and the wind luminosity of the cluster, $L_{\mathrm{w,c}} = \frac{1}{2}\dot{M}_{\mathrm{c}} v_{\mathrm{w,c}}^2$, which is determined by the mass-loss rate $\dot{M}_{\mathrm{c}}$ and wind speed $v_{\mathrm{w,c}}$. Expressions for R_s and R_b are given by equations (1) and (2) respectively.

$$R_s(t) = 48.6 \left(\frac{\rho}{\mathrm{cm}^{-3}}\right)^{-0.3} \left(\frac{\dot{M}_{\mathrm{c}}}{10^{-4}\mathrm{M}_\odot\mathrm{yr}^{-1}}\right)^{0.3} \left(\frac{v_{\mathrm{w,c}}}{1000\,\mathrm{km\,s}^{-1}}\right)^{0.1} \left(\frac{t}{10\,\mathrm{Myr}}\right)^{0.4} \mathrm{pc} \quad (1)$$

$$R_b(t) = 174 \left(\frac{\rho}{\mathrm{cm}^{-3}}\right)^{-0.2} \left(\frac{L_{\mathrm{w,c}}}{10^{37}\,\mathrm{erg\,s}^{-1}}\right)^{0.2} \left(\frac{t}{10\,\mathrm{Myr}}\right)^{0.6} \mathrm{pc} \quad (2)$$

The cold wind region between R_c and R_s is expected to have a constant wind velocity u_1, whereas in the shocked wind region between R_s and R_b the velocity is expected to drop $\propto r^2$. At the wind termination shock, the velocity becomes suppressed by a factor σ such that $u_2 = u_1/\sigma$. The full radial dependence of the cluster wind velocity is:

$$u(r) = \begin{cases} u_1 & r < R_s \\ u_2 \left(\frac{R_s}{r}\right)^2 & R_s < r < R_b \\ 0 & r > R_b \end{cases} \quad (3)$$

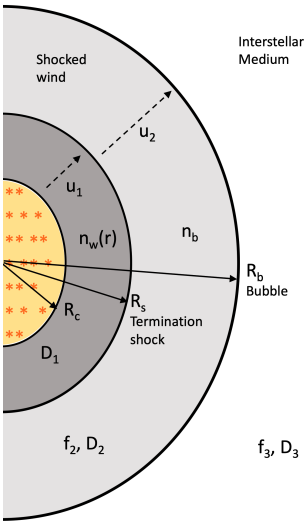

Figure 1: Schematic of the wind-blown bubble formed around a young stellar cluster, based on [2]. Subscripts 1, 2 and 3 refer to the cold wind, shocked wind and interstellar medium regions respectively.

Within the wind region, the density drops as $n_w \propto r^2$, whereas within the bubble, the density n_b is assumed constant and can be obtained from the mass-loss rate and the cluster age. To derive n_b, the total mass output by the cluster to date $\dot{M}_c t$, is assumed to be uniformly distributed throughout the bubble volume, $\frac{4}{3}\pi(R_b^3 - R_s^3)$.

Corresponding to these regions with distinct properties, we use diffusion coefficients D_1, D_2 and D_3 for the cold wind region, the shocked wind (bubble) and the ISM respectively.

3. Particle acceleration at the stellar cluster wind termination shock

Particle acceleration occurs at the wind termination shock, such that the particle distribution function $f_2(r, p)$ as a function of distance r and particle momentum p is:

$$f_2(r,p) = f_s(p) e^{\alpha(r)} \frac{1+\beta(e^{\alpha(R_b)}e^{-\alpha(r)}-1)}{1+\beta(e^{\alpha(R_b)}-1)} + f_{\rm Gal}(p) \frac{\beta\left(e^{\alpha(r)}-1\right)}{1+\beta(e^{\alpha(R_b)}-1)} \tag{4}$$

where $f_{\rm Gal}(p)$ takes the Galactic sea of cosmic rays into account in the overall particle distribution function within the bubble. The functions $\alpha(r, p)$ and $\beta(p)$ are:

$$\alpha(r,p) = \frac{u_2 R_s}{D_2(p)}\left(1 - \frac{R_s}{r}\right) \; ; \; \beta(p) = \frac{D_3(p) R_b}{u_2 R_s^2} \tag{5}$$

and $f_s(p)$ is the particle distribution at the termination shock:

$$f_s(p) = \frac{\chi_{\rm CR}}{2} \frac{\sigma n_1 u_1^2}{4\pi \Lambda_p (m_p c)^3 c^2} \left(\frac{p}{m_p c}\right)^{-s} e^{-\Gamma(p)} \, , \tag{6}$$

where $\chi_{\rm cr}$ is the CR acceleration efficiency, n_1 the wind numerical density, m_p the proton mass, $s = 4$ the spectral slope of acceleration, and Λ_p a normalisation constant. By fitting the pure

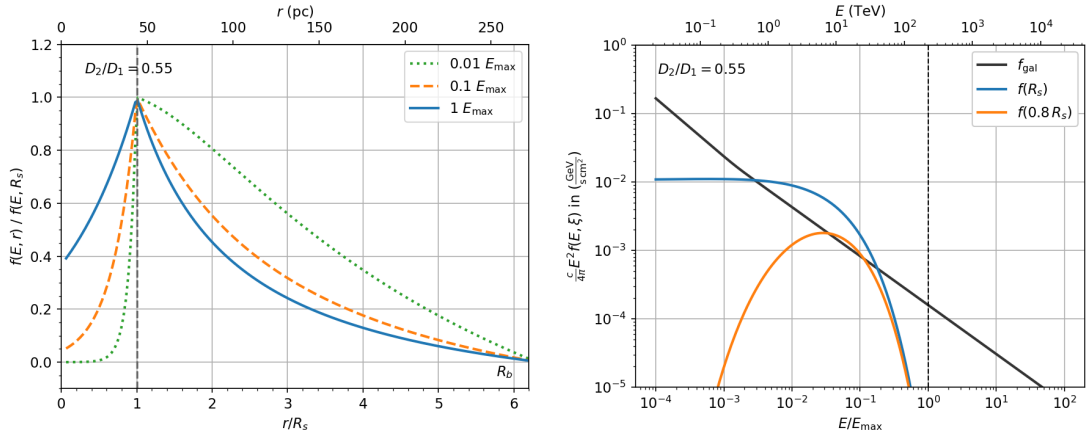

Figure 2: Particle distribution function of the stellar cluster wind. Left: the ratio of the particle distribution at a given energy to that at the wind termination shock R_s, as a function of distance from the shock. Right: the particle energy flux as a function of energy at R_s and just prior to R_s, compared to that for the sea of galactic CRs $f_{\rm gal}$.

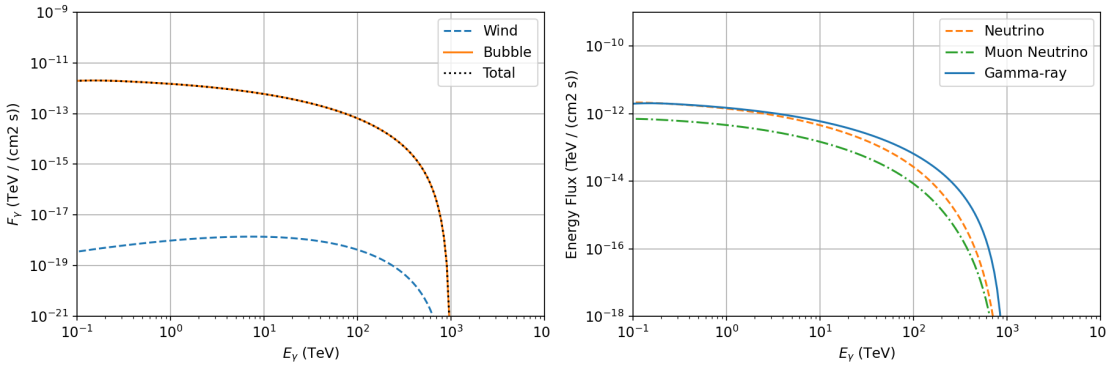

Figure 3: Left: γ-ray energy flux from different components of the stellar cluster environment. Due to the higher average density, the bubble dominates over the cold wind region. Right: Energy flux of secondaries produced via hadronic interactions.

exponential part of the solution with the following analytical expression:

$$\exp^{-\Gamma(p)} = (1 + A(p/p_m)^b) \exp^{-k(p/p_m)^c} , \tag{7}$$

we derive $k = 12.52$, $A = 5$, $b = 0.448549$ and $c = 0.064266$ for a Kraichnan-like diffusion coefficient, i.e. $D_1 = \frac{v}{3} r_L^{1/3} L_c^{2/3} \equiv k_1 p^{\delta_1}$ with $\delta_1 = 0.5$, v the particle velocity, r_L its Larmor radius, and $L_c \simeq 2$ pc the coherence length of the magnetic field. Finally, p_m can be obtained from the condition $D_1 = u_1 R_s$.

Figure 2 shows how the particle distribution function varies with distance and energy, where the ratio $f(r,p)/f(R_s,p)$ is set equal to unity at R_s. Within the bubble region, the particle distribution drops off more rapidly with distance for higher energies, and more slowly at lower energies. As a function of energy, the particle distribution at R_s provides the peak of the particle acceleration process.

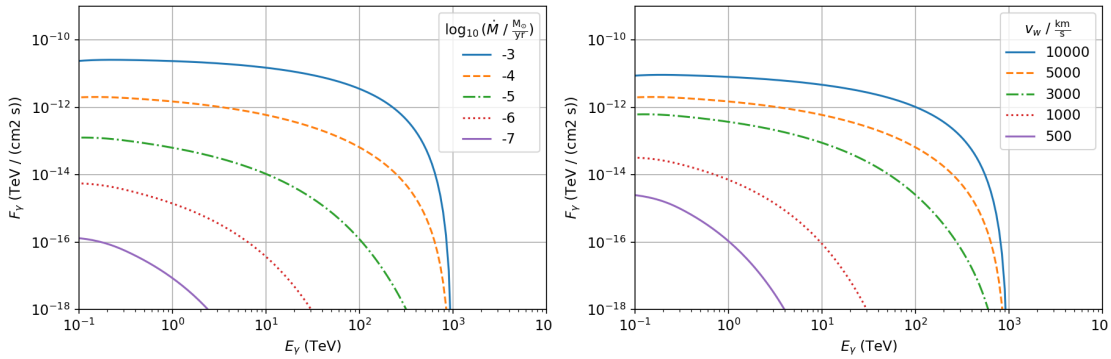

Figure 4: Variation in γ-ray energy flux with properties of the stellar cluster wind. Left: variation with mass-loss rate. Right: variation with wind velocity.

Figure 3 shows that as a consequence of the radial density profile of the cluster environment, the bubble region dominates the γ-ray emission from hadronic particles accelerated in the cluster wind. The average ambient density within the wind-blown bubble is assumed to be provided by an isotropic distribution of the integrated mass lost via the wind over the age of the stellar cluster. Hence, the contribution of the wind region to the total γ-ray flux is negligible. The energy flux of secondaries (neutrinos, gamma-rays) from the same parent particle population has a consistent shape over the energy range as also shown in Figure 3, where the muon neutrino flux is approximately one third of the all flavour neutrino flux [5].

4. Dependence of emission on stellar cluster properties

From the particle distribution functions given in equations (4) and (6), we obtain the γ-ray flux Φ_γ produced as these energetic particles interact with target material in the bubble region (of density n_b). Following the prescription of Kelner et al. [6]:

$$\Phi_\gamma(E_\gamma, R', t') = cn \int_{E_\gamma}^{\infty} \sigma_{\rm inel}(E) f(E, R', t') F_\gamma \left(\frac{E_\gamma}{E}, E \right) \frac{dE}{E} , \tag{8}$$

where we use the parameterisation of [7] for the inelastic cross-section $\sigma_{\rm inel}(E)$ for proton-proton interactions. Analogous expressions to (8) apply to evaluate the expected neutrino flux Φ_ν, using $F_\nu \left(\frac{E_\nu}{E}, E \right)$ in place of F_γ. Over long distances ($\gtrsim$ pc) the neutrino oscillation probabilities average to a constant, such that the flux of muon neutrinos is approximately one third that of the all-flavour neutrino flux [5]. Muon neutrinos are of particular interest, as they are the neutrino species which is most easily detected by modern neutrino experiments and with the most accurate direction reconstruction. Figure 3 shows the energy fluxes of secondaries (γ, ν and ν_μ) for a given (canonical) set of stellar cluster properties.

Figure 4 illustrates how the energy flux varies with mass-loss rate and wind velocity. As expected, both increasing $\dot{M}_c$ and increasing $v_{w,c}$ - corresponding to the wind luminosity - yield larger resulting γ-ray fluxes. With this model, we can determine which combination of properties will yield the most promising stellar cluster targets for detection by current and future experiments.

	Cluster	GLON (°)	GLAT (°)	Age (Myr)	Distance (kpc)	R_s (pc)	R_b (pc)	R_b (°)
1	Danks 2	305.390	0.089	2.0	2.2	45.8	181	4.63
2	NGC 3603	291.624	-0.518	1.0	7.2	32.5	115	0.92
3	Danks 1	305.342	0.074	1.0	1.9	31.6	113	3.45
4	Juchert 3	40.354	-0.701	1.0	1.5	25.7	98	3.80
5	DC 5	286.795	-0.502	1.1	4.4	25.9	103	1.33
6	Berkeley 59	118.230	5.019	1.3	1.0	24.5	103	5.87
7	NGC 6357	353.166	0.890	1.0	1.8	22.6	90	2.92
8	NGC 6611	16.962	0.811	2.1	1.6	28.5	134	4.66
9	Andrews Lindsay 5	27.733	-0.667	1.0	2.3	20.7	85	2.14
10	UBC 344	18.354	1.820	3.5	1.9	30.3	159	4.74

Table 1: Properties of the stellar clusters with the brightest predicted emission (integrated over the wind-blown bubble) in ranked order.

5. Predictions for emission from known stellar clusters

To obtain predictions for specific stellar clusters, we use the Milky Way Stellar Cluster (MWSC) catalogue and the open cluster sample from Gaia data release 2 [3, 4]. The energetics of stellar clusters are dominated by winds only within approximately the first 3 Myr, thereafter supernova remnant shocks start to contribute. Beyond ages of ~ 10 Myr, the cluster energetics can no longer be considered to be dominated by winds. Therefore, we applied selection criteria to the stellar clusters for which we evaluated the predicted γ-ray (and neutrino) energy flux. We required the clusters to be young, with an age < 10 Myr; to be compact, with a core radius (50% containment) less than the radius of the wind termination shock; and to have a reported effective temperature available, ensuring that a sufficient proportion of the member stars have been sampled by the respective catalogue.

For each stellar cluster in the selected sample, the required free parameters of the model (t, $\dot{M}$, v_w and n_b) could be either obtained directly from the catalogues or derived from known quantities.[1] This enabled the expected γ-ray emission to be evaluated using the model outlined above, together with the calculation of the expected R_s and R_b (see equations (1) and (2)). We sort the clusters according to the integral of the predicted γ-ray flux over the wind blown bubble and list the brightest ten in Tables 1 and 2. The corresponding spectral energy distributions are shown in figure 5.

Table 1 provides properties of these brightest ten clusters, amongst which the oldest (in tenth place) is UBC 344 with an age of 3.5 Myr, whilst all others are young with ages $\lesssim 2.1$ Myr. The wind termination shock radii are typically a few tens of pc, whilst the radii of the wind-blown bubbles are around $100 - 200$ pc, which - at distances ≤ 5 kpc, correspond to angular diameters of up to $\sim 10^\circ$ on the sky.

The spectral energy distributions for the ten clusters with the highest integrated energy flux above 1 TeV are shown in figure 5. It should be noted that given our model, the ranked order in terms of energy flux also corresponds to the ranked order in terms of the maximum energy. This

[1] Full details will be given in a forthcoming publication

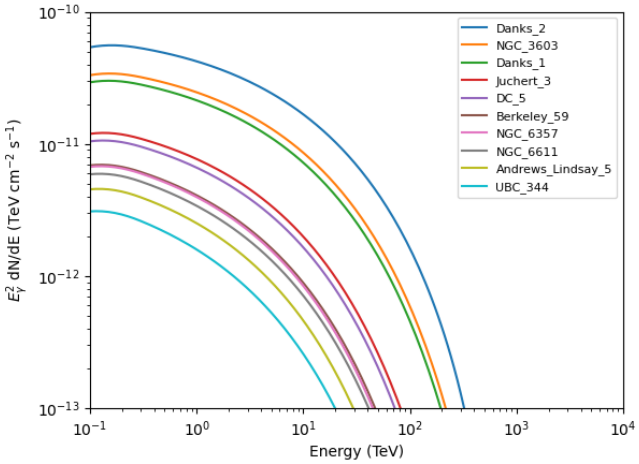

Figure 5: Stellar clusters with the brightest predicted γ-ray flux according to this model, integrated over the bubble region.

	Cluster	F_γ (> 1 TeV) (TeV cm^{-2} s^{-1})	$F_\gamma^{\rm ul}$ (> 1 TeV) (TeV cm^{-2} s^{-1})	$E_{\rm max}$ (PeV)
1	Danks 2	8.497e-11	1.217e-12	4.9998
2	NGC 3603	4.563e-11	2.446e-12	3.3612
3	Danks 1	3.887e-11	1.255e-12	3.1118
4	Juchert 3	1.208e-11	8.298e-12	1.7978
5	DC 5	1.02e-11	3.553e-12	1.6956
6	Berkeley 59	5.903e-12	–	1.3497
7	NGC 6357	5.669e-12	3.734e-12	1.2766
8	NGC 6611	4.822e-12	2.376e-12	1.3033
9	Andrews Lindsay 5	3.369e-12	3.063e-12	1.0146
10	UBC 344	2.021e-12	2.33e-12	0.8983

Table 2: Stellar clusters with the brightest predicted gamma-ray fluxes integrated above 1 TeV and properties, together with upper limits from the HGPS where available, corresponding to an angular size of 0.6°. Gamma-ray spectral energy distributions for the 10 brightest clusters are depicted in figure 5 [8].

can be seen in figure 5 and values for the maximum achievable energy, $E_{\rm max}$ are given in table 2. Despite all listed clusters achieving an $E_{\rm max} \gtrsim 1$ PeV, this is likely an overestimate as the influence of magnetic turbulence on the diffusion has not been taken into account, which would reduce $E_{\rm max}$.

Table 2 also provides the total integrated F_γ above 1 TeV over the whole wind-blown bubble, together with an upper limit extracted from the H.E.S.S. Galactic Plane Survey (HGPS) at the location of the stellar cluster yet with a radius of 0.6°. This is the largest angular radius out to which the HGPS data can be considered valid for the analysis of extended regions. Whilst in several cases the upper limits are lower than the predicted fluxes, due to the integration over the full bubble region (see Table 1) the surface brightness of these clusters will be much lower over an angular size of 0.6°.

The presence of target material such as molecular clouds in the vicinity of such an energetic particle population may act to enhance the detectable gamma-ray flux. Corresponding predictions, based on this model together with that of [9] and catalogues of known molecular clouds are given in a companion proceedings [10].

6. Conclusions

Several stellar clusters are predicted to have properties of PeVatrons according to the model applied in this study. Whilst the maximum energy achieved is likely a generous over-estimate, the predicted energy fluxes and $E_{\rm max}$ are promising for future observations. Nevertheless, the predicted emission is integrated over the wind-blown bubble, that may occupy a large region of space such that the surface brightness will be correspondingly reduced.

The detection of γ-ray emission from stellar cluster bubbles with angular sizes of the order of $\sim 6^\circ - 10^\circ$ will be challenging for Imaging Atmospheric Cherenkov Telescopes due to their limited field-of-view, however may be nevertheless detectable in suitably obtained survey datasets, and/or by virtue of the surface brightness profile, which will likely peak towards the wind termination shock (at much smaller radii than R_b). Survey instruments such as HAWC, LHAASO or the future SWGO are however well-suited to search for and study such extended sources. For the unambiguous detection of emission from bubble regions and association to stellar clusters, a robust treatment of source confusion effects and 3D analysis approaches will be of paramount importance.

Due to the hadronic processes, cluster environments producing bright γ-ray emission are also predicted to be strong neutrino emitters. Here, the large angular size of bubbles, may be beneficial, compared to the PSF of current and future generation neutrino instruments.

7. Acknowledgements

AM is supported by the Deutsche Forschungsgemeinschaft (DFG, German Research Foundation) – Project Number 452934793. SC gratefully acknowledges the support from Sapienza Università di Roma through the grant ID RG12117A87956C66.

References

[1] Z. Cao et al. [LHAASO Coll.], Nature **594** (2021) 33;
[2] G. Morlino, P. Blasi, E. Peretti & P. Cristofari, MNRAS **504** (2021) 6069;
[3] T. Cantat-Gaudin et al. [Gaia Coll.], A&A **640** (2020) A1;
[4] R. Kharchenko et al. A&A **558** (2013) A53;
[5] C. Mascaretti & F. Vissani, JCAP **08** (2019) 004;
[6] S.R. Kelner, F.A. Aharonian, V.V. Bugayov, Phys.Rev.D **74**, (2006) 034018;
[7] E. Kafexhiu, F. Aharonian, A. M. Taylor & G. S. Vila, Phys. Rev. D **90** (2014) 123014;
[8] H.E.S.S. Collaboration, A&A **612**, (2018) A1;
[9] A.M.W. Mitchell et al. MNRAS **503**, (2021) 3522;
[10] S. Celli et al. PoS(ICRC2023) **775** (2023)